PHYSICAL REVIEW B VOLUME 39, NUMBER 14 15 MAY 1989-I

Corrected effective-medium method. IV. Bulk cohesive and surface energies of second- and third-row metals and multilayer relaxation of Al, Fe, and Ni

Todd J. Raeker and Andrew E. DePristo
Department of Chemistry, Iowa State University, Ames, Iowa 50011

(Received 8 July 1988)

We provide a detailed analysis and discussion of the recently developed corrected effective-medium method (CEM) as applied to calculations of the bulk cohesive energies of the second- and third-row metals. The results demonstrate that a quantitatively accurate description of these quantities requires a new "covalent" embedding function instead of the self-consistent-field local-density "ionic" embedding function of Puska and co-workers. Construction of these covalent embedding functions from diatomic and bulk electron-density binding potentials is detailed. We present the formalism within the CEM method for the calculation of the surface energy of infinitely periodic two-dimensional solid surfaces. Calculations of the surface energies for the perfectly terminated low-Miller-index faces of Na, Mg, Al, K, Ca, Fe, Ni, and Cu are carried out. These results are compared to experimental measurements and very good agreement is found for almost all of these metals. More demanding multilayer surface-relaxation calculations are performed for Al(111), (110), and (100), Ni(110) and (100), and Fe(100). Very good agreement with experimental observations is obtained for these systems with the exception of Al(111) and (100). Detailed analysis of these calculations leads to an explanation of the relaxation process and its driving components.

I. INTRODUCTION

The experimental and theoretical study of metal surfaces has produced a wealth of information concerning the electronic and structural properties of metal surfaces. Of particular interest for the present paper are the geometric deviations of surfaces from that of the truncated bulk arrangement. Observations of large multilayer relaxations have been made for a number of systems such as Al(110) (Refs. 1 and 2) and Ni(110).[3–6] Smaller relaxations limited to the top surface layer have also been reported for Al(100),[7,8] Ni(100),[9] and Fe(100).[10]

First-principles self-consistent calculations using a local-density-functional formalism[11,12] have been carried out for a small number of systems, obtaining good agreement with experiment. These calculations, though accurate and very informative, are computationally very time consuming and difficult to carry out. Thus a large variety of simpler theoretical models[13–21] have also been developed in an attempt to predict and explain these dramatic deviations from that of the ideal surface. Some of these simplistic models are unable to predict accurately the magnitude and sometimes even the direction of the relaxation process. By contrast, the previously developed embedded-atom-method (EAM) of Daw and Baskes[22] has recently been applied to surfaces of fcc transition metals[23] and, though not self-consistent, produced relatively good agreement with experimental observations and measurements for surface energies and multilayer relaxations. In addition, the related effective medium (EM) theory[24,25] has been applied to the relaxation of Al surfaces[25] with some success.

Recently, three articles[26–28] (referred to as papers I–III) have been published, detailing the development and applications of the corrected effective-medium (CEM) method for the calculation of the interaction energies of small and large systems, including diatomic molecules, metal clusters, and bulk solids. In the present paper, we apply the CEM method to the calculation of the surface energy of a variety of metal surfaces. The CEM method is not entirely self-consistent, but it does, as will be discussed in Sec. III, have a basic component of self-consistency. Like the effective-medium theory, the CEM method begins by replacing the interaction energy of the multiatom system by the summation of the embedding energies for each atom in jellium having an effective electron density provided by the rest of the atoms in the system. The energy of embedding an atom in jellium is known from the self-consistent-field local-density (SCF-LD) calculations of Puska *et al.*[29] as a function of the homogeneous electron-gas density. In the CEM method one goes further by introducing and evaluating numerically the explicit *corrections* which describe the Coulombic-kinetic-exchange-correlation energies in the multiatom and jellium systems.

It is worthwhile to discuss briefly the relationship between the EM, CEM, and EAM methods. It is important to emphasize that the CEM formalism was not developed as an explicit correction to either of the other theories, but was derived from a consistent replacement of the fundamental relationship between the interaction energy of an N-body system and the embedding energy of each atom in jellium. The derivation is completely different from that of either of the EM or EAM theories. Nevertheless, by suitable approximations to the CEM formula, one can derive either EM or EAM theory. For EM, one neglects the correction for the kinetic-exchange-correlation energy, approximates the Coulombic correction via an induced-polarization formula, uses the SCF-

LD embedding functions, and uses a slightly different choice for the density of the jellium. For the EAM one also neglects the correction for the kinetic-exchange-correlation energy, replaces the Coulombic correction by an empirical function, uses empirical embedding functions, and uses a particularly simple choice of the jellium density. More details of these relationships can be found in papers I and II, with some further remarks in paper II.

One of the important points to come from paper II was that the embedding curve of Puska *et al.* reflects a rather ionic interaction of the atom with jellium. For homonuclear systems this is not quite correct and one should introduce another correction to reflect this fact. The form and implementation of this correction is still under active investigation, and at present a (semiempirical) covalent embedding function is used to replace the ionic interaction of Puska *et al.* in order to be quantitatively accurate for homonuclear systems. These curves were constructed from knowledge of the experimental diatomic binding curves in paper II.

In paper III the N-body formalism was derived for an infinitely periodic three-dimensional (3D) bulk metal system with one atom per unit cell. Applications to the binding in Mg_N and Cu_N clusters with $N=2,3,\ldots,13,19$ were presented. The covalent embedding functions for these two metals were constructed from knowledge of both the diatomic and bulk binding curves. It was suggested that these embedding functions were not functions of the number of atoms in the system, but instead were universal for any one type of atom in a homogeneous system.

The present article is divided into four sections. In Sec. II we derive the CEM-N relation for infinite systems with 2D translational symmetry (e.g., surfaces). In Sec. III we present calculated bulk cohesive energies for the metals of the second and third rows. The covalent embedding functions for Al, Na, K, Ca, Fe, and Ni are constructed. We then present and discuss results for the calculated surface energies of the perfectly terminated (111), (100), and (110) faces of these metals. Following this, the multilayer relaxation of Al(111), (100), (110), Ni(100) and (110), and Fe(100) is discussed in detail. Finally, Sec. IV contains a summary and conclusions of the method as applied to surfaces.

II. THEORY

The full details of the CEM method, especially CEM-N, are contained in papers I–III, to which the reader is referred. Here, we shall only present the features necessary to understand the extension and application to surfaces. The starting point is the interaction energy for a system of N atoms,

$$\Delta E(\{A_N\})=E\left[\sum_i A_i\right]-\sum_i E(A_i)\ , \tag{1}$$

which within the CEM-N formalism is rewritten in the equivalent form

$$\Delta E(\{A_n\})=\sum_i \Delta E_J(A_i;n_i)+\Delta V_c+\Delta G(\{A_N\})\ , \tag{2}$$

where all summations extend over the number of atoms in the system. The first term in Eq. (2) is the sum of the embedding energies in jellium of all the atoms of the system; two different types of embedding functions are considered in this paper and they are denoted the covalent, $\Delta E_C(A;n)$, and Puska *et al.*, $\Delta E_P(A;n)$, functions, respectively. The second term is the difference in Coulomb energy between the multiatom system and all the atoms in jellium. The last term is the difference in kinetic-exchange-correlation energy between the multiatom system and all the atoms in jellium, written as

$$\Delta G(\{A_N\})=G\left[\sum_i A_i\right]-\sum_i[G(A_i+n_i)-G(n_i)]\ , \tag{3}$$

where G denotes the sum of kinetic, exchange, and correlation energy functionals of the density, and n_i is the density of the jellium for the ith atom.

Equation (2) is not solved self-consistently, but instead utilizes the approximation of superposition of atomic densities to form the total system density. Minimizing the effect of this approximation on the non-selfconsistent ΔG term in Eq. (2) yields a prescription for the choice of the jellium density for each atom,[27] which for non-spin-polarized atomic densities is

$$n_i=\tfrac{1}{2}\sum_j(1-\delta_{ij})\langle n(\mathbf{r}_i)|n(\mathbf{r}_j)\rangle/Z_i\ . \tag{4}$$

The generalization to spin-polarized densities is presented in paper II, but this is not necessary for the present article. Here, $n(\mathbf{r}_i)$ is the unpolarized electron-density distribution and Z_i is the atomic number of atom i. Use of the superposition approximation simplifies the Coulombic correction ΔV_c to be the sum of the atom-atom Coulomb interactions.

Now, we invoke periodicity to simplify the evaluation of Eq. (2). The formalism for an infinite bulk system having 3D translational periodicity with one atom per unit cell has been presented previously[28] and thus will be merely outlined here. The cohesive energy is defined to be $E_{\mathrm{coh}}=\Delta E(\{A_N\})/N$ in the limit $N\to\infty$. Using the fact that all atoms in the system are equivalent in this limit, we can rewrite Eq. (2) for the cohesive energy as

$$E_{\mathrm{coh}}=\Delta E_J(A_b;n_b)+\Delta G_b+\tfrac{1}{2}\sum_{j\neq b}\Delta V_{jb}\ , \tag{5}$$

where ΔV_{jb} is the Coulomb interaction between atom j and the bulk atom b, and

$$\Delta G_b=G_b(\mathrm{bulk})-[G(A_b+n_b)-G(n_b)]\ . \tag{6}$$

The subscript "b" refers to any *one* of the bulk atoms. The evaluation of $G_b(\mathrm{bulk})$ involves an integral over the Wigner-Seitz cell of the atom A_b (see paper II). The task of calculating the energy of the infinite N-body system is now reduced to the calculation of the interaction energy of a bulk atom (A_b) in the electron-density environment due to the rest of the atoms in the metal.

In the case of surfaces, we can also simplify the evaluation of Eq. (2), but are restricted to use of 2D translational periodicity rather than the 3D periodicity in the bulk. Assuming no in-plane reconstruction, this periodicity implies that for surfaces we may consider the atoms within a particular layer as being equivalent (i.e., having the same electron-density environment). In this case we calculate the cohesive energy of *an atom in the ith layer as*

$$\Delta E_i = \Delta E_J(A_i;n_i) + \Delta G_i + \tfrac{1}{2}\sum_{j\neq i}\Delta V_{ij} \ . \tag{7}$$

To be more explicit, we pick a "focus" atom in layer i and calculate its cohesive energy via Eq. (7). The evaluation of ΔG_i entails a generalization to the simple integration over a Wigner-Seitz cell in the calculation of ΔG_b: the integration is over all spatial points which are closer to the focus atom "i" than to any other atom (just as in the general case for systems without any symmetry described in paper II).

For surfaces the fundamental quantity of interest is the surface energy, defined as $\sigma = [E(\text{bulk system}) - E(\text{two cleaved-surface systems})]/A_{\text{tot}}$, where A_{tot} is the total surface area. We can obtain this quantity by calculating ΔE_i for each layer leading into the bulk and by using the fact that $\Delta E_i \to E_{\text{coh}}$ as i gets larger. Since only one type of atom is considered here, there is only one atom per surface unit cell yielding the total surface area as $2N_s A$ for N_s surface atoms and unit cells each with area A. (Remember that two surfaces are formed from cleavage of one bulk system.) Combining this definition with Eq. (7) yields the final formula within the CEM formalism for the surface energy

$$\sigma = \sum_i (\Delta E_i - E_{\text{coh}})/A \ . \tag{8}$$

The summation over i extends over the *layers* and not over the individual atoms. To determine the extent of surface layer relaxation, we minimize the surface energy in Eq. (8) with respect to the displacement of one or more lattice planes in a direction perpendicular to the surface.

All that remains is to choose the energy-density functionals and the atomic densities. The kinetic-energy density functional used was a Padé summation of the gradient series[30] in $|\nabla n|/n^{4/3}$. The local Dirac exchange functional[31] and the local Gunnarson-Lundqvist[32] correlation-energy functional were used. As a representation of the atomic densities, we have generated an even-tempered Gaussian basis[33] from Slater-type atomic Hartree-Fock densities.[34] This allows convenient analytic evaluations of the Coulomb integrals and the density overlaps[35] [i.e., Eq. (4) for the jellium density]. Following paper II on diatomic molecules and subsequent (unpublished) studies by us of a variety of metals (uncluding those under study in the present paper), we utilized a non-spin-polarized atomic density since this yielded the most accurate energies within the CEM formalism. In addition, we have forced all the $3d$ transition metals to have a $(3d^n,4s^2)$ rather than a $(3d^{n+1},4s^1)$ configuration; it was seen in paper III that the semiempirical embedding function using two diffuse $4s$ electrons allowed for a much smoother match of the bulk and diatomic contributions to the curve. We have also restricted the $3d$ shell to be spherically symmetric, which has a negligible effect on the total electron-density distributions at the atomic separations of interest in this article.

III. RESULTS

A. Bulk metal cohesive energies

We have calculated the CEM bulk cohesive energies using the SCF-LD embedding functions of Puska *et al.* for the second- and third-row metals by minimizing Eq. (5) with respect to the lattice constant of the metal system. In the case of the hcp lattice, calculations were carried out by constraining the ratio c/a to that which is observed experimentally.[36] The atomic density around each atom was cut off at a radial distance such that $R^2\rho$ (where ρ is the atom density) $< 10^{-5}$ a.u. and all atoms within $2R$ of the focus atom were used to represent the infinite lattice. Inclusion of atoms outside this range and use of a larger cutoff radius resulted in negligible change in the calculated energies.

In Fig. 1(a) we show both the minimized CEM and experimental cohesive energies versus atomic number. A similar plot for the equilibrium nearest-neighbor distances (NND's) is shown in Fig. 1(b). For the second-row metals the CEM predictions are nearly quantitative for both the cohesive energies and NND's. However, for the third-row metals the situation is less satisfactory with predictions of the cohesive energy being accurate for $K \to V$ only and with predictions of the NND's all being contracted considerably, with the exception of K, where an expansion is predicted. Clearly there is some aspect of the interaction that is not described adequately using the embedding function of Puska *et al.* for the third-row metals.

We have further investigated the above problem by considering some relevant properties of atoms and jellium. First, we have also plotted the Pauling[37] electronegativity for the free metal *atoms* in Fig. 1(a), indicated as asterisks. An interesting correlation appears between the variation of the CEM calculated energies and the electronegativity as a function of the atomic number in each row. But this is not the sole reason for the inaccuracy of the functional of Puska *et al.* for the $3d$ elements, since even for Al and Si having relatively large electronegativities the predictions are still good. A second important point involves the variation of the work function for jellium, which is basically an increasing function from densities of 0 to 0.0018 a.u. with a peak of 2.4 eV, and then a linearly decreasing function of density thereafter, becoming negative after 0.0163 a.u. Figure 1(c) is a plot of the bulk jellium sampling densities for both the CEM and experimental NN distances as a function of the atomic number. One immediately notes that, in general, the density sampling increases as one proceeds across the second-row metals for both cases. For the transition metals we note that the density peaks at about V to Co and then decreases as the $3d$ shell is continually filled. From these considerations, the predicted results seen in Figs. 1(a) and 1(b) can be understood in terms of the overemphasis on an ionic interaction inherent in the SCF-LD embedding curve of Puska *et al.* for an electronegative atom in a high-density jellium system.

Let us consider the above points in more detail. For the second-row metals the density sampled by the atoms

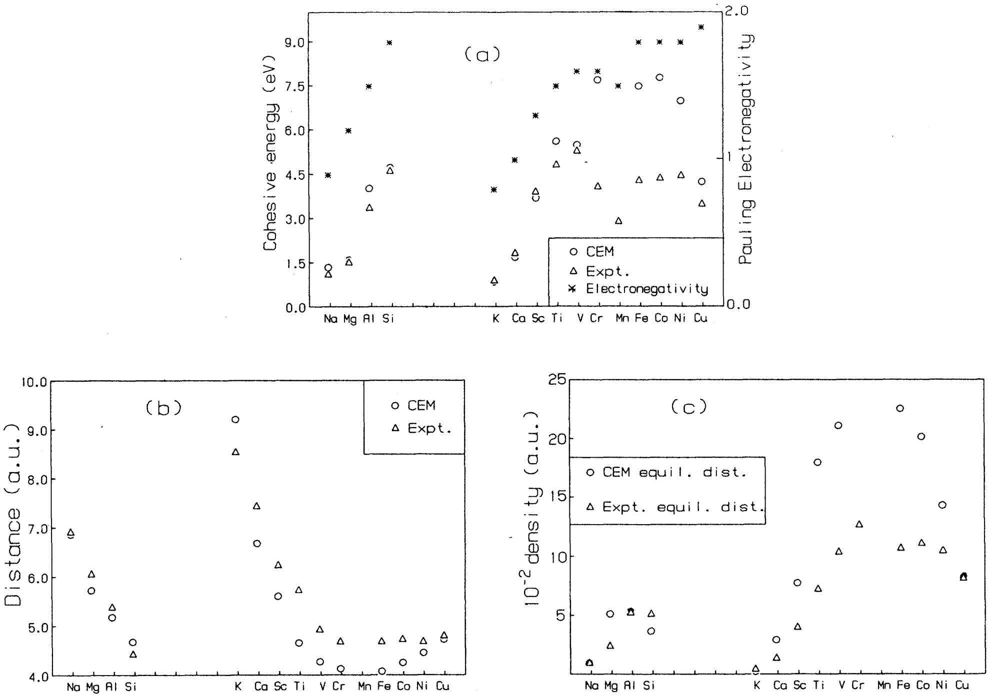

FIG. 1. Calculated bulk metal cohesive energies and nearest-neighbor distances along with the experimental values (Ref. 36) are shown. Also, Pauling's free-atom electronegativity (Ref. 37) is plotted for a comparison of ionic characteristics of the embedding functions. (a) CEM and experimental cohesive energies. Electronegativities are symbolized by asterisks. (b) CEM and experimental nearest-neighbor distances. (c) Sampled jellium densities at the CEM and experimental equilibrium distances.

in the bulk is relatively low and thus the work function of jellium is high, ensuring that the degree of ionic interaction is small. This results in the general agreement found with experiment for both the cohesive energy and the NN distance. In the case of the third-row metals for Ti to Cu the sampling density is considerably larger, resulting in a lowering of the work function of jellium. Therefore one would expect the ionic interaction with jellium to be significant and that the use of the functional of Puska *et al.* will predict a substantial ionic component to the bonding, especially for the right-half transition metals. Since the experimental trend in binding energy does not follow the CEM predictions, we must conclude that a substantial ionic bonding component is not correct. These results support our initial argument in the theoretical section that in order to obtain quantitative binding energies an alternative embedding function must be used. The use of a corrected embedding function will allow us to adequately describe the correct type of interaction occurring on clean metal surfaces.

B. Covalent embedding functions

Paper II presented semiempirical covalent embedding functions which were constructed solely by inverting the experimental binding potential curves for homonuclear diatomics. These covalent embedding functions are determined by solving Eq. (2) (with $J=C$) for $\Delta E_C(A;n)$,

$$\Delta E_C(A;n)=[\Delta E(A_2)-\Delta G(A_2)-\Delta V_c(A_2)]/2 \ . \qquad (9)$$

For $\Delta E(A_2)$ a Morse-potential representation of the experimental data[38] was used. Following paper III, we also utilize the bulk cohesive energy to determine the covalent embedding function via Eq. (5):

$$\Delta E_C(A;n)=E_{\text{coh}}-\Delta G_b-\tfrac{1}{2}\sum_{j\neq b}\Delta V_{jb} \ . \qquad (10)$$

In this analysis the bulk experimental binding potential is obtained from a harmonic expansion about the equilibrium lattice constant with the bulk modulus providing the second derivative of the cohesive potential. Table I contains the experimental data used to construct the bulk portion of the embedding functions for the atoms considered in this paper. Included in this table is the bulk data for other metals for which we have constructed covalent embedding functions but which are not discussed in this paper. Once the two portions of the embedding curves are constructed they are combined to form one covalent embedding function that we propose will be universal with respect to the number (N) of atoms in the system of a particular element as applied with the CEM approach.

This universality implies that the effects of all other variations with number of atoms in the system are incorporated into the Coulombic and correction terms. The latter is particularly important to discuss since the reader may question the requirement of a correction term

TABLE I. Cohesive energies and lattice constants calculated from Eq. (5) using the embedding functions of Puska *et al.* (Ref. 29).

	CEM			Experiment[a]		
	a (a.u.)	E_{coh} (eV)	Structure	a (a.u.)	E_{coh} (eV)	Bulk modulus[b] (10^{11} N/m^2)
Na	7.94	1.38	bcc	7.98	1.113	0.68
Mg	5.76	1.62	hcp[c]	6.07	1.53	3.54
Al	7.35	4.05	fcc	7.65	3.39	7.22
K	10.65	0.88	bcc	9.87	0.934	0.32
Ca	9.49	1.71	fcc	10.54	1.84	1.52
Fe	4.75	7.52	bcc	5.42	4.28	16.83
Ni	6.32	7.00	fcc	6.65	4.44	18.6
Cu	6.72	4.26	fcc	6.82	3.50	13.7
Si[d]	10.88	4.76	dia[e]	10.25	4.63	9.88
Sc	5.63	3.66	hcp	6.25	3.90	4.35
Ti	4.68	5.62	hcp	5.74	4.85	10.51
V	4.98	5.52	bcc	5.73	5.31	16.19
Cr	4.79	7.71	bcc	5.44	4.71	19.01
Co	4.27	8.80	hcp	4.74	4.39	19.14

[a] All experimental values obtained from Ref. 36.

[b] The bulk modulus provides the second derivative for the harmonic expansion of the cohesive energy in construction of covalent-embedding function.

[c] The ratio c/a was held constant for hcp structures.

[d] The surface energies or relaxation of the metals below the space are not studied. Thus a covalent embedding function is not constructed in this paper for these metals. The Mg and Cu functions were constructed in paper III.

[e] The diamond lattice structure was used for Si.

(which is time consuming to compute) when the embedding functions are determined semiempirically. First, note that the correction term is determined by the spatial variation of the electron density, becoming small as a system becomes more homogeneous. In particular, the correction is most important for diatomics and becomes rather small for bulk systems (both assumed to be near the equilibrium distance). In contrast, the embedding energy (per atom) is smallest for diatomics and becomes rather large for bulk systems due to the increasing number of neighbors. Thus, the correction term cannot be incorporated into a semi-empirical embedding function. To test this argument, we have determined new embedding functions in exactly the same manner as described above but without the correction term; the results for the surface energies and relaxations were considerably poorer than those in which the correction term is retained (and which will be presented in Sec. II C). For transition-metal surface energies, including relaxation, typical errors are on the order of 5% with the correction energy and 20% without the correction energy. These quantities are rather sensitive to the difference in inhomogeneity of the electron density between bulk and surface atoms. For quantities which may not be so sensitive to such inhomogeneity (e.g., composition of bimetallic systems or even the desorption energy of a surface metal atom), it may be possible to eliminate the correction term.

We illustrate the construction of semiempirical embedding function by providing a step-by-step analysis for the construction of the covalent embedding function for Al. The embedding curves for the rest of the metals will simply be presented and discussed since the construction procedure is the same for all atoms.

In Fig. 2(a) we have plotted the harmonic binding potential for bulk Al as a function of both the lattice constant and the sampled jellium density. Figure 2(b) is an analogous plot for the binding potential of Al_2. The five points shown in Fig. 2(a) correspond to lattice constants of 90%, 95%, 100%, 105%, and 110% of the experimental equilibrium lattice constant. In Fig. 3, we have plotted the covalent embedding function resulting from the application of Eqs. (9) and (10) to this data. The embedding function of Puska *et al.* for Al is also shown. Only the high-density (90%→105%) bulk points were retained since the true binding curves are expected to be softer than harmonic for the very expanded low-density geometries. These points correspond to the four points labeled to the left of and including the point indicated by an arrow in Fig. 2(a) and with the corresponding embedded energies labeled $N=\infty$ in Fig. 3. The diatomic points for bond lengths less than the point indicated by the solid square in Fig. 2(b) were not retained since the Morse potential is not expected to be accurate in this region. The two vertical arrows in the low- and high-density regions of Fig. 3 indicate the location of the diatomic and bulk densities on the embedding curves corresponding to the experimental equilibrium bond distance and lattice constant, respectively.

Examination of these figures demonstrates that the diatomic and bulk systems correspond to separate regions of

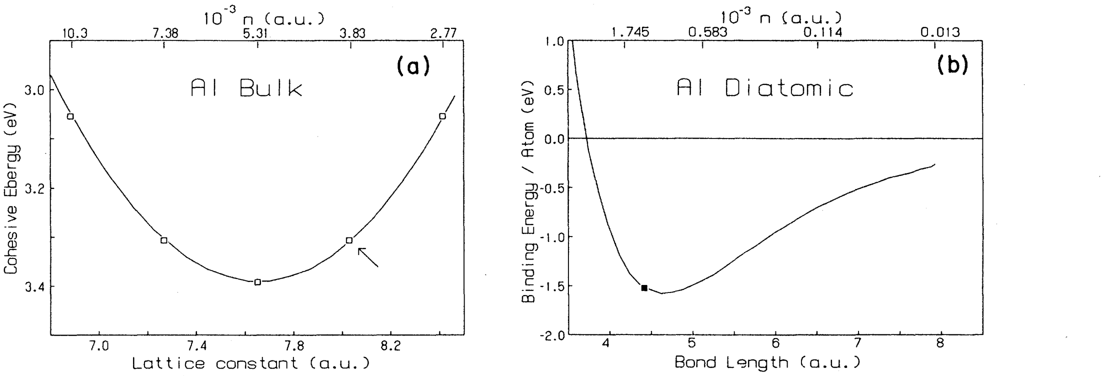

FIG. 2. The experimental potentials for Al (from which the Al semiempirical covalent embedding function is derived) are plotted as a function of both the internuclear spacing (lattice constant for the bulk; bond length for the diatomic) and the corresponding sampled jellium density *n*. (a) Bulk metal. (b) Diatomic molecule.

sampled density. Hence, the smoothness of the interpolation between these two regions provides strong evidence for the *universality* of the covalent embedding curve. One should also note the excellent qualitative agreement between the two embedding curves in Fig. 3. The two differ by a constant for almost all densities with the curve of Puska *et al.* lying below the covalent curve. This is characteristic, as seen in paper II, of a partial ionic interaction for the (partially negative) charged atom in jellium. The fact that the slopes are almost the same is reflected in the excellent agreement of the Al NND in Table I with experiment. Another important distinction between the two embedding curves is that the embedding function of Puska *et al.* is drawn to the negative of the electron affinity of the free atom in the zero-embedding-density limit,[29] while the covalent embedding function is drawn to zero. This will be the case for all atoms with a positive electron affinity.[24,29]

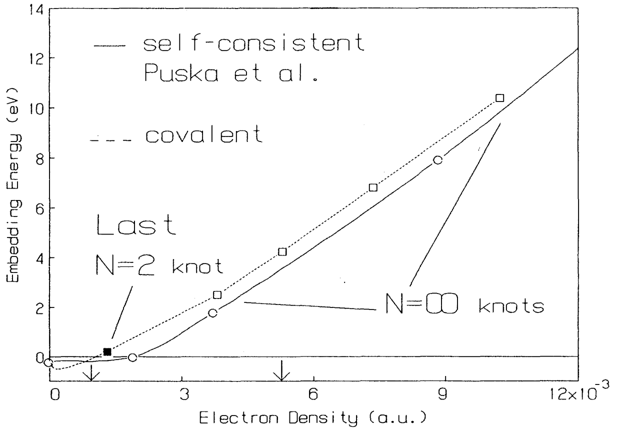

FIG. 3. The semiempirical covalent embedding function (squares) for Al is shown. Also shown is the SCF-LD embedding function (open circles) as calculated by Puska *et al.* (Ref. 29). The embedding energy is plotted as a function of the jellium density. The vertical arrows in the low- and high-density regions indicate the location of the equilibrium diatomic and bulk points, respectively.

Carrying out the same procedure for Na, we show in Fig. 4 both the Puska *et al.* and the covalent embedding functions. In this case only the three highest bulk-electron-density points were used in order to obtain a smooth fit and, as can be seen, even this leaves a somewhat nonsmooth curve. This will be seen later to lead to difficulties in accurately calculating the energies of Na surfaces. In comparison to Al, we find that the Na embedding function of Puska *et al.* is closer to the covalent curve throughout the whole density range, indicating that Na is slightly less negative in jellium. This is expected since not only is the electronegativity of Na lower, but the sampled electron density is also much lower, yielding a higher jellium work function. Also note that there is only one calculated Puska *et al.* embedding energy point in this lower-density region.

For K we show in Fig. 5 both the Puska *et al.* and resulting covalent embedding curves. The bulk points in this case were also truncated at the 100% lattice value. Although the curve of Puska *et al.* is slightly *above* the covalent curve, this is not of concern since the embedding

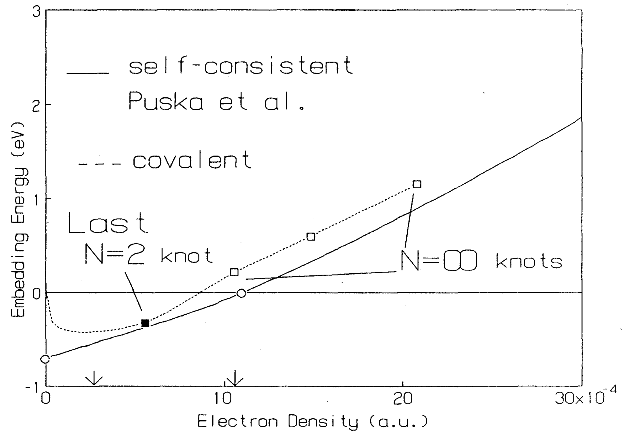

FIG. 4. Same as Fig. 3, except for Na.

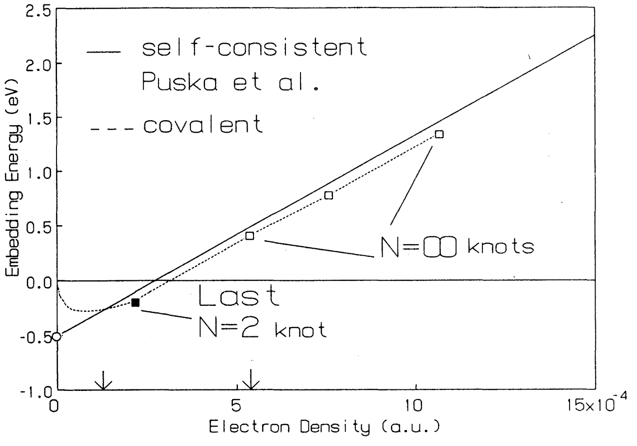

FIG. 5. Same as Fig. 3, except for K.

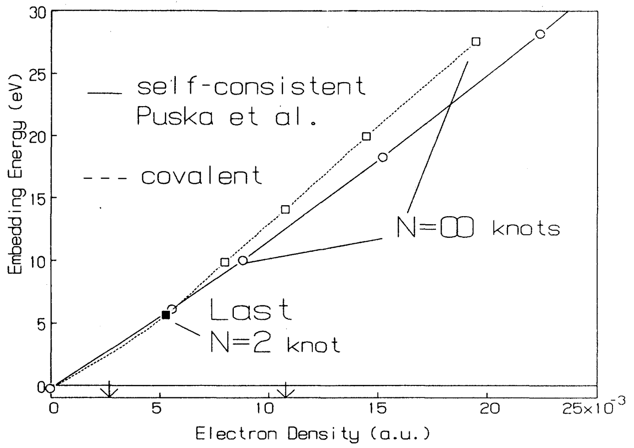

FIG. 7. Same as Fig. 3, except for Fe.

function of Puska *et al.* in this region is an extrapolation from a calculated high-density point to the negative of the electron affinity, and is thus quite uncertain. With no real data points this region of the embedding curve is unknown self-consistently and thus the covalent embedding function not only provides the correct type of interaction, but it also fills in the gap in the calculations of Puska *et al.* This also indicates that the calculated bulk cohesive energy and NN distance shown in Figs. 1(a) and 1(b) for K should not be taken very seriously.

In the case of Ca, we see in Fig. 6 a smooth curve again with truncation at the 100% bulk lattice point. Like K, the embedding curve of Puska *et al.* for Ca is very slightly above the covalent curve and is mainly an extrapolation in the zero density limit. As in the case of K, the covalent embedding function fills in the gap in the embedding function of Puska *et al.*

Moving now to Fe, we see in Fig. 7 that in the covalent embedding curve smooth interpolation between the diatomic and bulk regions is quite remarkable. We were able to retain many more diatomic points (e.g., note the last diatomic point relative to the first vertical arrow) without any loss of smoothness. We were even able to retain the 105% lattice value in the bulk region as well. We also see a dramatic transition in the ionic character of Fe in jellium indicated by the increasing separation of the covalent and Puska *et al.* embedding curves as the density is increased. The increased density results in a lower work function for jellium, suggesting that Fe is slightly negative in jellium at such densities. Since there are a number of Puska *et al.* points in the region of interest, the bulk calculation can be considered reliable.

Finally, we examine the embedding functions of Ni in Fig. 8. We see that the covalent embedding function is above that of the embedding function of Puska *et al.* throughout the whole range of densities, in contrast to that seen in Fe. Even though they both have the same electronegativities, the Ni atom has a greater tendency to fill its 3*d* shell than Fe does. In the case of Ni, we had to truncate again the high-density diatomic and low-density (> 100%) bulk contributions to the embedding curve to obtain a smooth interpolation of the diatomic and bulk

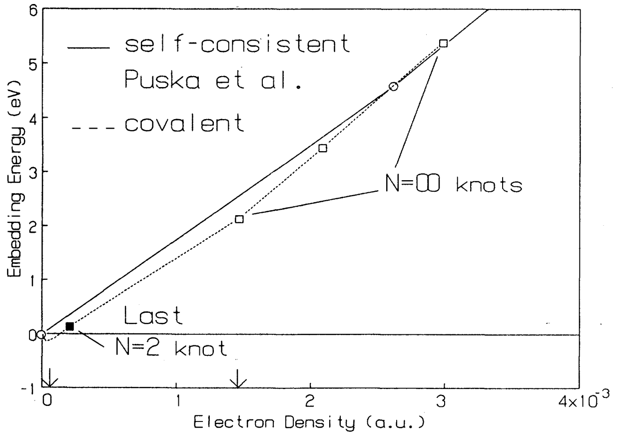

FIG. 6. Same as Fig. 3, except for Ca.

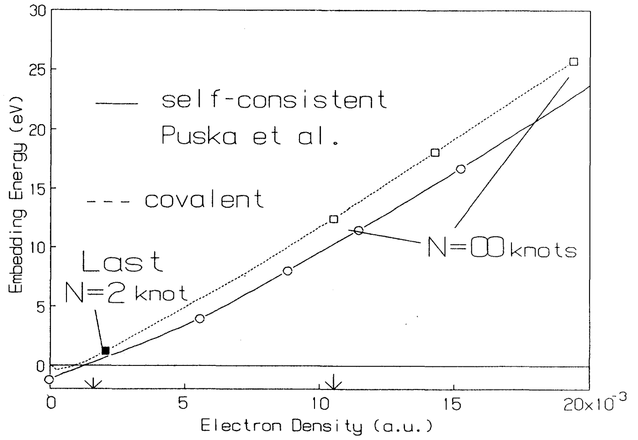

FIG. 8. Same as Fig. 3, except for Ni.

regions. Again, the bulk calculation can be considered reliable, as there are plenty of Puska *et al.* points in this region.

The covalent-embedding functions of both Cu and Mg were presented in paper III, where the same procedures as above were carried out. The characteristics seen for these two metals are very similar to Ca for Mg and Ni for Cu. In the case of Cu the Puska *et al.* and covalent embedding function were very close, indicating only a very small ionic interaction of Cu in jellium.

C. Surface energies and relaxation

As described previously, an accurate calculation of the bulk cohesive energy and lattice constant requires the use of the covalent embedding functions. With these functions at hand, we can predict a number of properties of the metal, and in this subsection we have calculated the surface energies of a number of perfectly terminated low-Miller-index faces of Na, Mg, Al, K, Ca, Fe, Ni, and Cu from Eqs. (7) and (8). Later, we will consider the multilayer relaxations of a select few of these surfaces, but we emphasize that the surface energy is only slightly affected by such relaxation.

As in the calculations for bulk systems, the total number of atoms must be large enough such that the electron density sampled by the focus atom in each layer is unaffected by the addition of more atoms. In addition, for surfaces, the summation in Eq. (8) over the energy of each layer must be converged with respect to the number of layers. For the closely packed surfaces, it was found that only four layers were needed for convergence of Eq. (8) to be obtained while, for more open surfaces, five to six layers were needed. In all cases the total number of layers in the system was constrained to $2n+1$, where n is the number of focus layers indicated above. This ensured that the energy of the nth focus atom was equal to E_{coh} within numerical accuracy.

Before discussing the results, we feel that a few general points concerning the various contributions to the surface energy is in order. First, we expect the embedding-energy contribution to be negative since the embedding-energy repulsion is smaller due to the lowered electron density at the surface relative to the bulk. This also implies that the more open the surface is, the more negative this contribution will become. Second, we expect that the Coulombic contribution will be positive and dominant since the surface atoms have completely lost the longer-range electrostatic interactions with the atoms above the plane of the surface. Note also that the more open surfaces will have a larger Coulombic energy contribution than the more closely packed surfaces. The trend of the correction-energy contribution is difficult to predict, but we do expect that it will be relatively small for the simple free-electron-like metals.

In Table II we show the CEM predictions for the surface energies along with its energy components (with obvious notation) for the low-index faces of various metals. Due to the unavailability of experimental data on isolated surface planes, direct comparison is only semiquantitative[39]. In general, though, very good agreement with experiment is obtained for almost all of these metals, and if the experimental data are assumed to be mainly for the most close-packed surfaces, the predictions are nearly quantitative. One also notes immediately the difference in magnitudes for the simple metals as compared to the transition metals. Also, as expected, the trend of increasing surface energy with increasing openness of the surface is seen for these cases. During the calculations we also noted that the contributions to the total surface energy arose from deeper layers for the more open surfaces. This trend agrees with the experimental finding that multilayer relaxations can occur for the open surfaces, while for the more closely packed surfaces the relaxation is limited to the top layer and, in some cases, the second layer as well. We shall have more to say about this aspect of the surface energy and relaxation.

In comparison to the variational jellium with ion-core pseudopotential model results of Sahni *et al.*,[40] we note that agreement is not very good for Na, Al, and K, where CEM consistently underestimates the surface energy. This is especially true for Na and K. Even then, recall that their calculations were a variational treatment of the surface and thus would represent an upper limit on the surface energy of these simple metals. Comparison to the embedded-atom-method calculations[23] that included planar relaxation for Ni and Cu shows that EAM considerably underestimates the surface energy. EAM can be considered a simpler CEM method without the correction term and with parametrized forms for the homogeneous and Coulombic energy terms. Since σ_{cor} is negative, its neglect would increase σ_{tot}, and thus the errors in EAM must come from parametrizing the homogeneous and Coulombic energies.

Of the metals studied in this paper, the cases of Na and K show calculated surface energies that are in significant disagreement with both experiment and the work of Sahni *et al.* To understand why this occurs, we examined more closely the embedding-energy contributions and noted that the top-layer atoms of any metal sample a jellium density that is between the last diatomic point and the first bulk point as seen in Figs. 3–8 of the embedding functions. As mentioned in Sec. III. B this area of the embedding curve is the least known due to the unavailability of experimental data for systems that would have sampling densities in this region. With this in mind, a quantitatively accurate calculation of surface energies would support confidence in the universality of the embedding function.

For Na we find that the jellium density for the top-layer atoms correspond to a point just below the upward hump of the embedding curve, thereby causing the embedding energy for these atoms to be artificially lowered relative to the bulk. This lowered embedding energy would result in a more negative surface-energy contribution and thus tend to lower the total surface energy for sodium. Because of this, we feel that in order to accurately describe the Na surfaces, we need to have a much smoother embedding function in this region of the surface density. This nonsmoothness, we believe, may be a result of the restriction to nonpolarized atom densities,

TABLE II. Calculated surface energies and energy components in J/m^2 of the low-index-surface faces.

	CEM				Other	
	$\sigma_{E_{\rm hom}}$	σ_{V_c}	$\sigma_{\rm cor}$	$\sigma_{\rm tot}$	theory	Expt.[a]
Na (100)	−0.484	0.570	0.053	0.139	0.270[b]	
(110)	−0.407	0.484	0.069	0.147	0.248[b]	0.261
(111)	−0.437	0.583	0.048	0.158	0.305[b]	
Mg(1000)	−1.403	1.999	0.048	0.643	0.629[b]	0.785
Al (100)	−4.061	5.456	−0.160	1.230	1.701[b]	
(110)	−4.275	5.812	−0.183	1.353	2.964[b]	1.143
(111)	−3.732	4.938	−0.110	1.096	0.852[b]	
K (100)	−0.306	0.383	0.013	0.090	0.161[b]	
(110)	−0.270	0.322	0.029	0.081	0.147[b]	0.145
(111)	−0.304	0.386	0.013	0.095	0.176[b]	
Ca (100)	−0.866	1.461	−0.017	0.578	0.615[b]	
(110)	−0.920	1.563	−0.020	0.622	0.737[b]	0.578
(111)	-0.795	1.307	0.010	0.523	0.472[b]	
Fe (100)	−14.970	17.537	−0.135	2.429		
(110)	−12.651	15.245	−0.105	2.489		2.417
(111)	−15.106	17.978	−0.181	2.690		
Ni (100)	−13.106	15.935	−0.207	2.622	1.580[c]	
(110)	−13.935	17.073	-−0.259	2.878	1.730[c]	2.380
(111)	−11.899	14.596	−0.135	2.561	1.450[c]	
Cu (100)	−9.731	11.775	−0.321	1.722	1.280[c]	
(110)	−10.350	12.551	−0.388	1.813	1.400[c]	1.790
(111)	−8.756	10.640	−0.259	1.625	1.170[c]	

[a] Average of a polycrystalline surface, Ref. 39.

[b] Variational jellium calculations with weak ion pseudopotentials for nuclear core roles from Ref. 40.

[c] Embedded-atom-method results from Ref. 23.

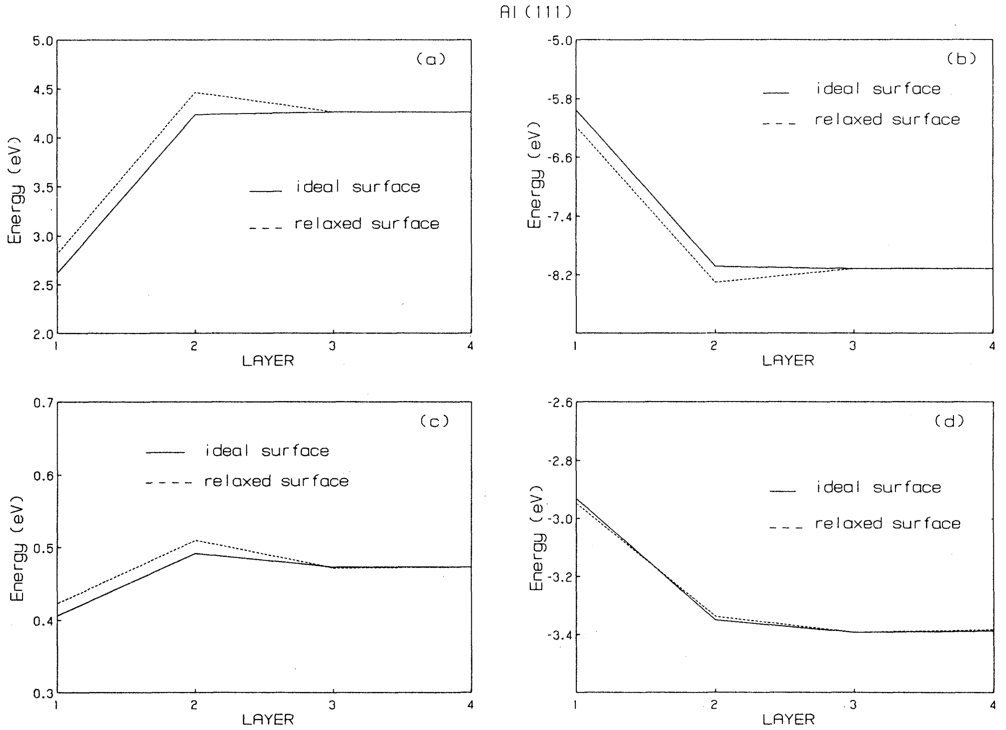

FIG. 9. The energy components for the ideal and relaxed Al(111) surface as a function of the layer are shown. (a) Homogeneous embedding energy. (b) Coulombic energy. (c) Correction energy. (d) Sum of components $a+b+c$.

which will be more severe for low-atomic-number atoms. By contrast, for K such nonsmoothness for the embedding function does not occur. But we do note that the correction-energy contribution is significantly less for K than it is for Na, and the magnitude of the difference between the experimental and CEM results is not very large.

For the rest of the metals there are no dramatic deviations from experiment. We see that the Coulombic contribution to the surface energy is indeed dominant and that the correction-energy contribution is nonnegligible ($\approx 10-20\,\%$ of σ_{tot}) and negative for the more inhomogeneous transition metals, and also surprisingly for Al as well.

Now we examine in detail the multilayer relaxations of some of the surfaces studied above. The more closely packed surfaces will be studied first leading into more open surfaces where large relaxations are expected to take place and to extend deep into the subsurface layers.

The Al(111) surface has been studied experimentally a number of times with nearly all results indicating an expansion of only the top layer, with values ranging from $\Delta d_{12}=3\pm2\%$ (Ref. 41) to $\Delta d_{12}=0.5\pm0.5\%$.[42] There is one instance where a very large contraction, $\Delta d_{12}=-7.7\pm2\%$, has been observed.[8] A recent theoretical study[18] has reported a slight contraction, $\Delta d_{12}=-0.4\%$, while we have found a larger top-layer contraction, $\Delta d_{12}=-3.0\pm1\%$. To see if an expansion is possible for this surface, we allowed small expansions of the first interlayer spacing, but this always yielded a larger surface energy compared to the ideal surface.

In Figs. 9(a)–9(d) we show a plot of the CEM energy components $[\Delta E_C(\mathrm{Al};n)$, $\frac{1}{2}\Sigma_j\Delta V_{ij}$, ΔG_i, and the sum] for each layer atom from Eq. (9) for the ideal and contracted surface of Al(111). Examining these plots, one notes immediately that the largest changes as a result of the contraction are in the embedding and Coulomb energies. The embedding energy becomes more repulsive due to the increased electron density during contraction, but at the same time the Coulombic attraction between these layers increases due to the decreasing separation. Also, note that the correction energy in Fig. 9(c) ends up being slightly more repulsive for this surface indicating that the electron-gas density is more inhomogeneous after contraction has occurred. The potential per layer atom shown in Fig. 9(d) indicates that even though the individual energy components change significantly during relaxation, these changes tend to cancel. Indeed, the minimized surface energy for the contracted geometry is 1.076 J/m^2 compared to 1.096 J/m^2 for the ideal surface. This change in surface energy is so small that it pushes the limits of precision of our calculations. In view of this difficulty, a smaller contraction certainly could be possible. For larger changes in the surface energy, this will not be a problem, and it will be seen next that the slightly more open (100) surface falls into this category.

We show in Table III the results of the multilayer relaxation of Al(100) in comparison to experimental values. The correct direction of relaxation is predicted, but again the magnitude is much larger than is observed experimentally. Also, note that we find that the second interlayer distance has significantly expanded, where the experimental study seemed to have not taken into account or observed a possible relaxation of this spacing. To see if this expansion effects the top-layer contraction, we allowed only the top layer to relax with the result being the same, $\Delta d_{12}=-5.0\%$ contraction, indicating that for this surface the magnitude in relaxation of the top layer is independent of the relaxation of the second or deeper interlayer distances.

In Fig. 10 we show the components of the energy contribution to the cohesive energy for each layer atom. For the top two layers, the embedding energy has increased, but the expansion of the second interlayer spacing leads to a significantly lower electron density for the third-layer atoms, which results in a lowering of their embedding energy. The analogous behavior is also apparent for the Coulomb and correction energies. Note that the magnitude for these changes in the first and third layers are almost the same, but opposite in direction. Inspection of Fig. 10(c) shows that the correction energy has increased with relaxation for the top two layers and then has decreased dramatically for the third layer. The increased repulsion seen in the correction for the first two layers seems to be a characteristic of Al surfaces and will be seen later to reflect the lack of 3d electrons.

TABLE III. Multilayer percent of bulk relaxation of Al(100), Fe(100), and Ni(100).

	Al			Fe		Ni	
	CEM	expt.	EM[a]	CEM	expt.	CEM	expt.
Δd_{12} (%)	-5.0	-2.2[b]	-3.0	-1.5	-1.5[c]	-3.5	-3.2[d]
Δd_{23} (%)	$+3.5$	0.0	0.0	$+0.5$	0.0	$+2.0$	0.0
Δd_{34} (%)	$+0.5$	0.0	0.0	0.0	0.0	0.0	0.0
σ_I[e]	1.230			2.461		2.621	
σ_R[f]	1.158		0.830	2.399		2.320	

[a] Reference 25.

[b] This is an upper limit to the contraction as provided in Ref. 8. In Ref. 7 a value of -1.5% is reported.

[c] Reference 10.

[d] Reference 9.

[e] Surface energy for the ideal surface, in J/m^2.

[f] Surface energy for the relaxed surface, in J/m^2.

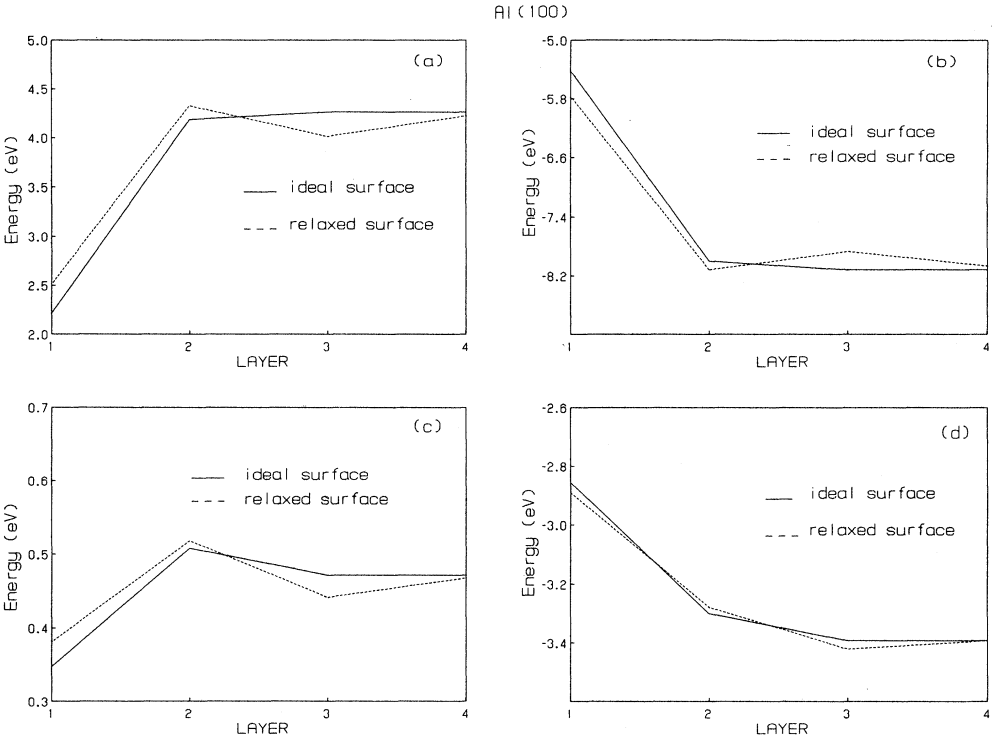

FIG. 10. Same as Fig. 9, except for Al(100).

Although the change in the surface energy is not very large in total, the variation in the potential per layer is much larger than for Al(111). From Fig. 10(d) we see that the potential has been lowered in the top- and third-layer atoms. The contraction between the first two layers results in a lower first-layer potential, while the second-layer potential is raised, and the latter is lowered again by expanding the distance between the second and third layers. This decrease in interaction does not, however, raise the potential of the third layer over that of the ideal surface, but on the contrary is more stable after relaxation. Closer inspection shows that while the expansion between the third and second layers has decreased the attractive Coulomb interaction, it has also decreased the embedding energy by a slightly larger amount. This feature along with the decrease in the correction energy for this layer accounts for most of the lowering in the layer potential. Through these plots we are able to see a simple picture of the oscillatory behavior of the relaxation process beginning to appear.

Next, we show in Table III the results of the multilayer relaxation of Fe(100). We find very good agreement with experiment but, as can be seen, the change in the surface energy is small enough that the accuracy of the calculations might be in question. Indeed, during the analysis the surface energy oscillated a considerable amount within this range and it was found that an expanded first interlayer distance was more favorable than the ideal surface, but not the contracted surface. Examination of Fig. 11 shows that all the energy components remain essentially constant during the contraction, and therefore not much can be said about this surface.

We also show in Table III the results of the multilayer relaxation of Ni(100), finding very good agreement with experimental results. While $\Delta d_{12} = -3.5\%$ in both studies, we find a corresponding expansion of 2.0% for the second interlayer spacing. The experimental study did not mention this possible expansion, and when only the top layer was relaxed, we still obtained $\Delta d_{12} = -3.5\%$. This indicates that, as in Al, the relaxation of the top layer seems to be rather independent of the relaxations of other layers in the subsurface. The energy of relaxation for this surface is very large, and thus the results can be considered very reliable since this energy is well outside the precision limits of the calculations.

In Fig. 12 we show the energy components for this surface as a function of layer. As a result of the contraction, we see the expected increase in the embedding energy for the top two layers, and also the expected corresponding decrease for the third-layer atoms due to the expansion. The Coulomb energy shows the same trend as Al(100), but now the correction energy decreases upon relaxation for all the layers, in contrast to the oscillatory behavior that is seen for the same Al face. Despite this difference the potential in Fig. 12(d) again reveals the oscillatory behavior of the relaxation process as explained in detail for the Al(100) surface.

Earlier we mentioned that the increase in ΔG_i with decreasing Δd_{12} for the first two layers in Al(111) and Al(100) was due to the lack of d electrons. To confirm this we removed the $3d$-shell electrons from Ni by contracting them into the nucleus, thereby reducing the

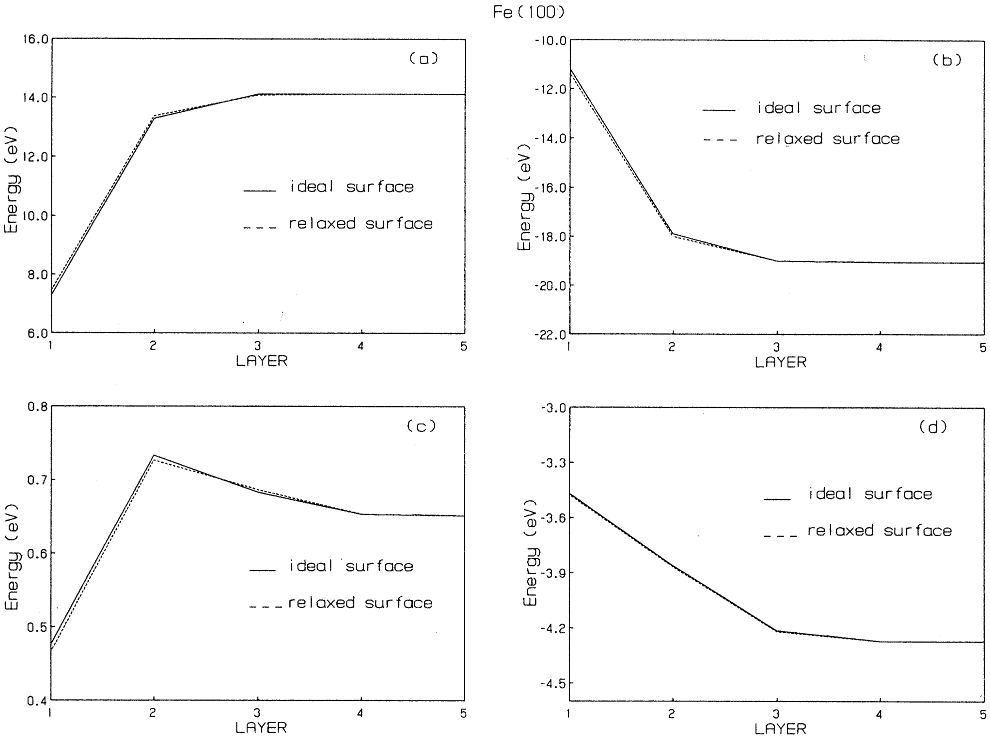

FIG. 11. Same as Fig. 9, except for Fe(100).

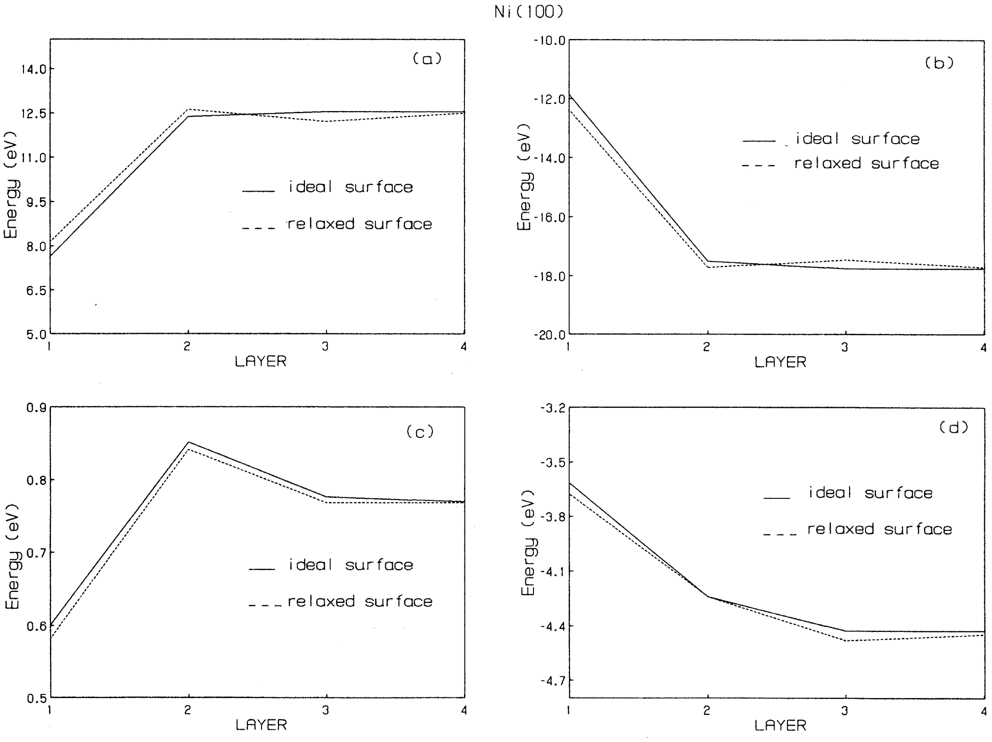

FIG. 12. Same as Fig. 9, except for Ni(100).

atomic number by eight. Using the embedding function of Puska *et al.*, we found $a = 7.3$ bohrs and $E_{\mathrm{coh}} = 2.8$ eV resulting in an expanded and weakly bound solid. This clearly indicates the significant bonding nature of the $3d$ electrons. Calculations for the ideal and relaxed surfaces showed that the correction energy now increases upon relaxation and exhibits the oscillatory behavior as observed in the Al surfaces. This indicated that the $3d$ electrons are an important factor in the difference between the relaxation process in simple versus transition-metal surfaces. A similar finding occurred if we did not use the embedding function of Puska *et al.* but instead created a new covalent-embedding curve using the same experimental diatomic and bulk data as before in Sec. III B.

Returning to computations of surface relaxations, we consider the more open fcc (110) surface for both Al and Ni. The ideal surface energy seen in Table II is much larger than for the fcc (100) face, and thus we expect the multilayer relaxations to be more pronounced. In Table IV we present the CEM results for Al(110) in comparison to experimental data and theoretical EM (Ref. 25) and SCF-LD (Ref. 12) calculations. We obtain very good agreement with experiment and relatively good agreement with the self-consistent calculations for all interlayer spacings. In comparison to the EM values, we find that CEM is more sensitive to the relaxation process and that the surface energy of the relaxed surface is much more in agreement with that seen by the SCF-LD calculations and experiment. The energy of relaxation is small but, keeping in mind that the surface area of the unit cell is quite large, is none the less large enough to lie outside the precision limits in the calculations.

During the analysis we also allowed only the top layer to relax obtaining a $\Delta d_{12} = -10\%$ contraction, again indicating that the top-layer relaxation is relatively independent of other interlayer relaxations. The situation is quite different for the remaining layers where large correlations between the relaxations were observed. The relaxation of the second interlayer spacing was difficult to determine without a corresponding contraction of the third interlayer spacing, which, in turn, was dependent on the fourth interlayer spacing expansion. Basically, since the surface is so open, the interactions between layers becomes more sensitive to changes in the local environment of atoms in each layer.

The above correlation can best be seen by examination of Fig. 13. The embedding energy shows an increase for the top layers, but a decrease for the third and fourth layers. In contrast, the Coulomb energy is nearly constant after the first two layers, while the correction energy decreases after the first two layers. The plot of the potential in Fig. 13(d) again reveals the oscillatory behavior of the relaxation process. When the top layer contracts so much, the second layer responds by increasing d_{23} in order to greatly decrease its interaction with the third layer. Now the third- and fourth-layer atoms compensate for this loss of interaction by contracting the third interlayer spacing. This cycle continues in a decreasing manner as the layers progress inward towards the bulk.

For the relaxation of Ni(110), we present in Table IV a summary of the results from CEM in comparison to experimental data. As in the case of Al(110), we obtain excellent agreement for the top two layers, whereas the relaxations for the third and fourth layers were either not experimentally studied or not detected in the Ref. 4, while in Ref. 43 a very small contraction of the third interlayer spacing was reported. The calculated relaxation process showed a similar correlation between the relaxation of the layers as observed in Al(110). A plot of the energy components for Ni(110) is shown in Fig. 14, and comparison to Fig. 13 for Al(110) shows qualitatively similar features for both the embedding and Coulomb energies in the top two layers, with differences beginning in the third layer. The embedding energy for the third layer in the relaxed geometry is now larger than that of the ideal surface for Ni(110), whereas the opposite is true for Al(110). This feature may be a result of a smaller expansion in the third interlayer spacing for Ni(110) than in Al(110). The most striking difference though lies in the correction energy, whereas all the layers in Ni(110) lower their respective correction energies as a result of the relaxation. This is equally true for the third and fourth lay-

TABLE IV. Percent of bulk multilayer relaxation of Al(110) and Ni(110).

	Al(110)				Ni(110)		
	CEM	SCF-LD[a]	EM[b]	Expt.[c]	CEM	Expt.	
Δd_{12} (%)	-9.5	-6.8	-7.0	-8.6 ± 0.8	-9.5	$-9.0^{d}\pm1.0$,	-8.7^{e}
Δd_{23} (%)	$+5.5$	$+3.5$	$+1.0$	$+5.0\pm1.1$	$+4.0$	$+3.5\pm1.5$,	$+3.0$
Δd_{34} (%)	-1.5	-2.0		-1.6 ± 1.2	-1.5		-0.5
Δd_{45} (%)	$+1.0$	$+1.6$			$+1.0$		
σ_I[f]	1.353	~1.2			2.879		
σ_R[g]	1.265	-1.09	0.883		2.592		

[a] Reference 12 indicated relaxation energy of ≈10 meV.

[b] Reference 25.

[c] Reference 1.

[d] Reference 4.

[e] Reference 43.

[f] Surface energy for the ideal surface, in J/m^2.

[g] Surface energy for the relaxed surface, in J/m^2.

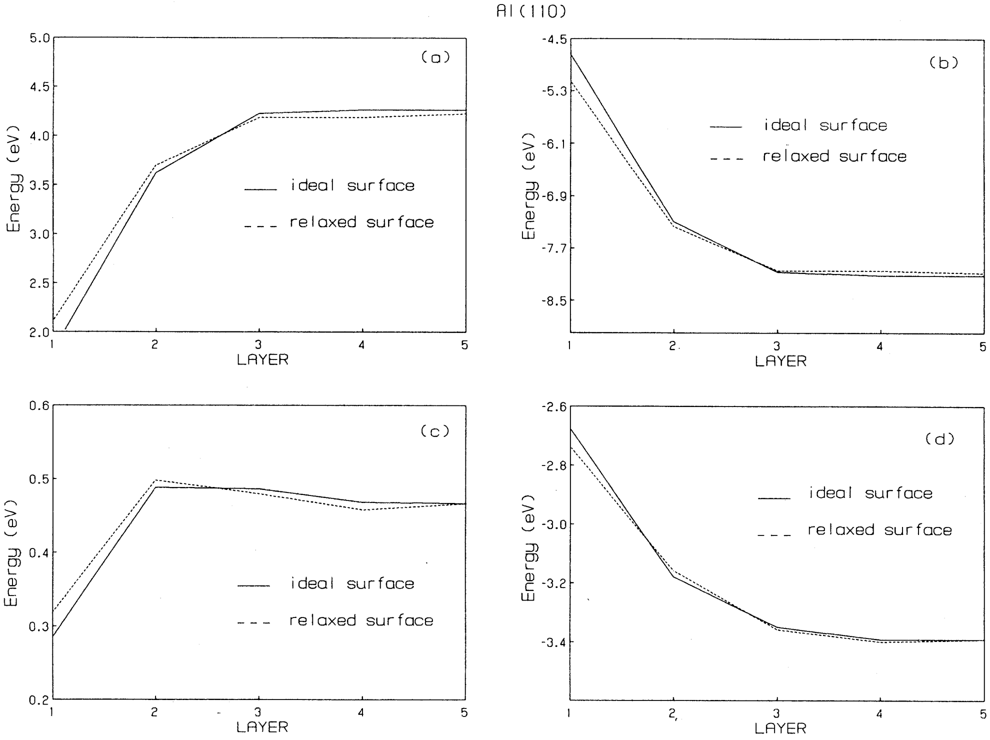

FIG. 13. Same as Fig. 9, except for Al(110).

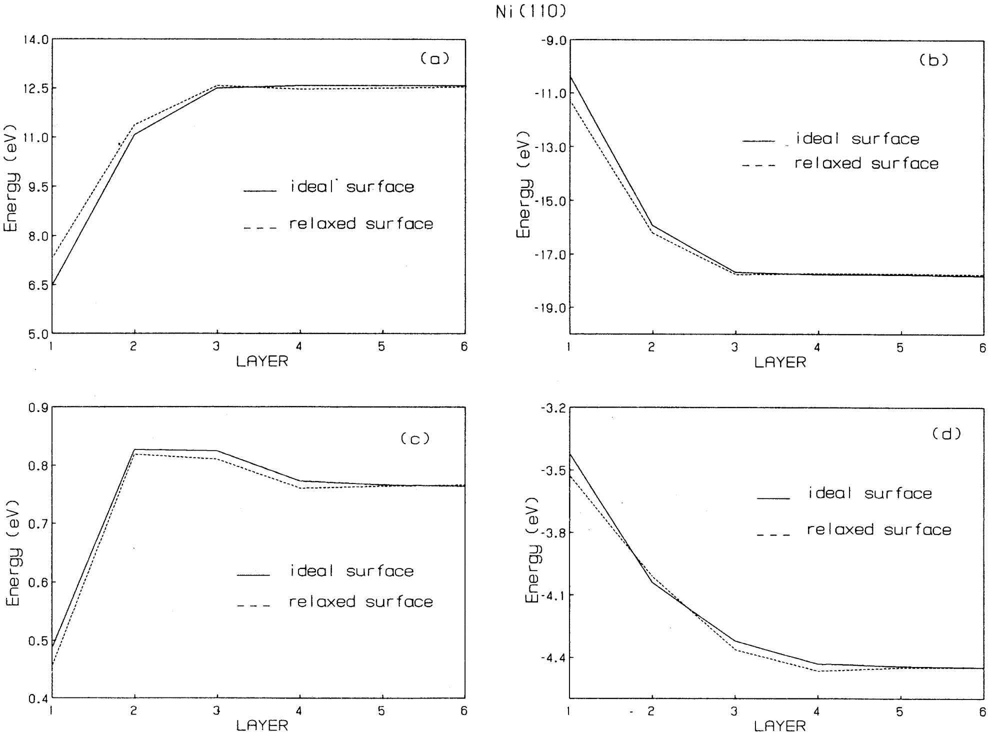

FIG. 14. Same as Fig. 9, except for Ni(110).

ers. The resulting sum of the energy components yields the potential in Fig. 14(d). We see that the top-layer potential is lowered while the second layer stays relatively stable. But surprisingly, the third and fourth layers give significant contributions to the relaxation process as reflected by their respective potentials.

With the above calculations we can now draw some important conclusions about the multilayer relaxation process. We have seen that the top-layer contraction is independent to a significant degree of the relaxation of the rest of the layers below it. In contrast, the second interlayer spacing expansion (if it is relatively large) is highly dependent upon the relaxation (contraction) of the third-layer spacing. This feature of the relaxation process can most likely be extended to the rest of the simple and transition metals and studies are underway to determine if this is indeed true.

IV. SUMMARY AND CONCLUSIONS

Calculated cohesive energies for the second- and third-row metals were presented using the corrected-effective-medium (CEM) method with the embedding functions of Puska *et al.* for the atoms in jellium. It was shown that these embedding functions do not provide an accurate description of the type of bonding occurring for such homonuclear systems. In an attempt to describe the correct type of interaction, we have constructed (semiempirical) covalent embedding functions using both the experimental diatomic binding potential and bulk cohesive energies. These two different types of systems determined different parts of the covalent-embedding curve, and a smooth interpolation between the two was obtained. This feature supported the postulated universality of this embedding energy as a function of the size of the system. It was also seen that for the electropositive atom the covalent embedding energy is lower than the ionic energy of Puska *et al.* This is in contrast to characteristics of the electronegative atoms studied in paper II where the covalent embedding energy is larger than that of the values of Puska *et al.*

We have presented the formalism for the calculation of the surface free energy of an infinitely periodic 2D metal surface within the CEM method. Within this method, we used the covalent embedding functions to calculate the surface energy for a number of second- and third-row metals. The energies were shown to agree very well with experimental measurements and to predict the correct qualitative trend of increasing surface energy with increasing openness of the surface. We then carried out multilayer relaxation calculations of well-known surfaces through minimization of the surface energy. Very good agreement was obtained for most of the surfaces studied. In our opinion these calculations are, in general, consistently more accurate and complete than those of other models presented to date in their ability to correctly describe the stability and structural features of various metal surfaces at modest computational expense [e.g., determination of an energy for Ni(110) required 125 min of central-processing-unit time on a RIDGE 3200 computer, which is approximately 3 times faster than a VAX 11/780].

With the ability to accurately describe the metal surface, calculations are currently being carried out to determine the effect on relaxation of various chemisorbed atoms as a function of the coverage. These results will be presented in a future publication.[44] Also, the method is being extended to include more complicated in-plane reconstructions of the metal surface. Improvements in computational methodology are being implemented which may greatly increase the speed of this method to the point where simulations of crystal and cluster growth and roughening may become feasible. If fundamental extensions can be developed to allow for a nonempirical correction between covalent and ionic bonding embedding functions, the CEM approach offers the real possibility of a consistent, accurate, and fast computational scheme for the determination of the interaction energies of a collection of different types of atoms ranging from heteronuclear diatomics to large clusters of hundreds of atoms to bulk solids.

ACKNOWLEDGMENTS

This work was supported by National Science Foundation (NSF) Grant No. CHE-86-09832. One of us (T.J.R.) is very pleased to acknowledge many beneficial conversations with Dr. Joel D. Kress. A.E.D. acknowledges partial financial support from the Camille and Henry Dreyfus Foundation and the Alfred P. Sloan Foundation.

---

[1] J. N. Anderson, H. B. Nielson, L. Peterson, and D. L. Adams, J. Phys. C **17**, 173 (1984).

[2] J. R. Noonan and H. L. Davis, Phys. Rev. B **29**, 4349 (1984).

[3] Y. Gauthier, R. Bauding, C. Gaubert, and L. J. Clark, J. Phys. C **15**, 3223 (1982); **15**, 3231 (1982).

[4] Y. Gauthier, R. Bauding, Y. Joly, C. Gaubert, and J. Rundgren, J. Phys. C **17**, 4547 (1984).

[5] D. L. Adams, L. E. Peterson, and C. S. Sorenson, J. Phys. C **18**, 1753 (1985).

[6] S. M. Yalisove, W. R. Graham, E. D. Adams, M. Copel, and T. Gustafsson, Surf. Sci. **171**, 400 (1986).

[7] N. Masud, R. Bauding, D. Abedam, and C. Gaubert, Surf. Sci. **133**, 580 (1983).

[8] A. Bianconi and R. Z. Bachrach, Phys. Rev. Lett. **42**, 104 (1974).

[9] J. W. M. Frenken, J. F. van der Veen, and G. Allan, Phys. Rev. Lett. **51**, 1876 (1983).

[10] R. Imbihl, R. J. Behm, and G. Ertl, Surf. Sci. **123**, 129 (1982).

[11] C. L. Fu, S. Ohnishi, E. Wimmer, and A. J. Freeman, Phys. Rev. Lett. **53**, 675 (1984).

[12] K. M. Ho and K. P. Bohnen, Phys. Rev. B 6 **32**, 3446 (1985).

[13] G. Allan and M. Lannoo, Surf. Sci. **40**, 375 (1973).

[14] R. N. Barnett, U. Landman, and C. L. Cleveland, Phys. Rev. B **28**, 1685 (1983); Phys. Rev. Lett. **51**, 1359 (1983).

[15] T. Halicioglu, H. O. Damuk, and S. Erkoc, Surf. Sci. **143**, 601 (1984).

[16] R. A. Johnson, Surf. Sci. **151**, 311 (1985).
[17] D. Tománek and K. H. Bennemann, Surf. Sci. **163**, 503 (1985).
[18] P. Jiang, P. M. Marcus, and F. Jona, Solid State Commun. **59**, 275 (1986).
[19] M. Manninen, Phys. Rev. B **34**, 8486 (1986).
[20] A. G. Equiluz, Phys. Rev. B **35**, 5473 (1986).
[21] X. W. Wang and W. Weber, Phys. Rev. B **35**, 7404 (1987).
[22] M. S. Daw and M. I. Baskes, Phys. Rev. B **29**, 6443 (1984).
[23] S. M. Foiles, M. I. Baskes, and M. S. Daw, Phys. Rev. B **33**, 7983 (1986).
[24] J. K. Norskov and N. D. Lang, Phys. Rev. B **21**, 2136 (1980); M. J. Stott and E. Zarembra, *ibid.* **22**, 1564 (1980).
[25] K. N. Jacobson, J. K. Nørskov, and M. J. Puska, Phys. Rev. B **35**, 7423 (1987), and references therein.
[26] J. D. Kress and A. E. DePristo, J. Phys. **87**, 4700 (1987).
[27] J. D. Kress and A. E. DePristo, J. Chem. Phys. **88**, 2596 (1988).
[28] J. D. Kress, M. S. Stave, and A. E. DePristo, J. Phys. Chem. **93**, 1556 (1989).
[29] M. J. Puska, R. M. Nieminen, and M. Manninen, Phys. Rev. B **24**, 3037 (1981); M. J. Puska (private communication).
[30] A. E. DePristo and J. D. Kress, Phys. Rev. A **35**, 438 (1987).
[31] A. E. DePristo and J. D. Kress, J. Chem. Phys. **86**, 1425 (1987); J. P. Perdew, Phys. Rev. Lett. **55**, 1665 (1985); A. D. Becke, J. Chem. Phys. **84**, 4524 (1986); S. K. Ghosh and R. G. Parr, Phys. Rev. A **34**, 785 (1986); O. Gunnersson, M. Johnson, and B. I. Lundqvist, Phys. Rev. B **20**, 3136 (1979).
[32] O. Gunnarsson and B. I. Lundqvist, Phys. Rev. B **13**, 4274 (1976).
[33] M. Schmidt and K. Ruedenberg, J. Chem. Phys. **71**, 3951 (1979).
[34] E. Clementi, IBM J. Res. Dev. Suppl. **9** (1965); P. S. Bagus, T. L. Gilbert, and C. J. Roothan, J. Chem. Phys. **56**, 5159 (1972).
[35] S. Huzinaga, Prog. Theor. Phys. Suppl. **40**, 279 (1967).
[36] C. Kittel, *Introduction to Solid State Physics* (Wiley, New York, 1986).
[37] L. Pauling, *The Nature of the Chemical Bond* (Cornell University Press, Ithaca, NY, 1960), p. 93.
[38] K. P. Huber and G. Herzberg, *Constants of Diatomic Molecules* (Van Nostrand, New York, 1979).
[39] W. R. Tyson and W. A. Miller, Surf. Sci. **62**, 267 (1977).
[40] V. Sahni, J. P. Perdew, and J. Gruenebaum, Phys. Rev. B **23**, 6512 (1981).
[41] F. Soria, M. C. Munuz, and J. L. Sacedon, Surf. Sci. **128**, 424 (1983).
[42] H. B. Nielson and D. L. Adams, J. Phys. C **15**, 615 (1983).
[43] D. L. Adams, L. E. Petersen, and C. S. Sorensen, J. Phys. C **18**,1753 (1985).
[44] T. J. Raeker and A. E. DePristo (unpublished).